Chapter 4

Lipid-Coated Nanocrystals of Paclitaxel as Dry Powder for Inhalation: Characterization, *In-Vitro* Performance, and Pharmacokinetic Assessment

Chapter 4. Lipid-Coated Nanocrystals of Paclitaxel as Dry Powder for Inhalation: Characterization, In-Vitro Performance, and Pharmacokinetic Assessment

4.1. Rationale

Paclitaxel (PTX) being one of the most effective anticancer drugs, has been employed in treating lung cancer. It works by stabilizing the microtubules of cells and inhibiting the late G2 or M phases of the cell cycle, causing cells to die. However, PTX has poor aqueous solubility, limiting the clinical application. Although PTX has been formulated using Cremophor EL (brand name "Taxol") consisting of castor oil and dehydrated ethanol to overcome solubility issues, it showed serious adverse effects such as allergic reactions. Solvent Cremophor EL also alters the drug kinetics, leading to non-linearity (Wang et al., 2017). PTX also suffers from drug resistance due to P-gp efflux, which decreases the intracellular concentration of the drug. Therefore, the design of a novel formulation free of Cremophor EL is required to improve aqueous solubility and mitigate drug-related adverse effects.

Fucoidan stabilized nanocrystals (FPNCs) with high drug payload and hydrophilic surface can be formulated and subsequently be coated with phospholipids to produce Lipo-NCs mimicking lung surface. Lipo-NCs acts as novel drug delivery system integrating drug nanocrystals into hydrophilic core of liposomes to form a hybrid system. Lipo-NCs offer advantage of both nanocrystals (high drug loading, enhanced dissolution, and improved aerosolization stability) as well as lipid-nanoparticles (colloidal stability, membrane fluidity, controlled drug release, and surface modification) (Kumar et al., 2020a; Liang et al., 2021). The Lipo-NCs can provide prolonged drug retention, lower drug clearance and high gradient concentration in lung (He et al., 2020b, 2023a). The nanocrystals can be used as dry powder for inhalation (DPIs) with excellent aerosolization performance, facilitating homogenous particle

distribution and deposition to deep lungs. This can result in maximum drug localization in lungs available for uptake by lung cancer cells and also avoids drug distribution to other major organs, thereby providing better therapeutic effect and avoiding systemic side effects.

4.2. Objective

Formulation of a dry powder for inhalation of fucoidan stabilized and lipid-coated nanocrystals. Nanocrystals were investigated for particle size, zeta potential, encapsulation efficiency, and drug loading. Nanocrystals were also characterized using various microscopy and spectroscopic techniques to confirm formation of fucoidan-stabilized nanocrystals and lipid-coated nanocrystals. In addition, wettability, saturation solubility, in-vitro drug release, in-vitro mucous diffusion, powder flow property, and aerosolization studies were conducted to determine their efficiency in drug delivery. Pharmacokinetic and biodistribution study were also done for confirming in-vivo performance and drug delivery potential of prepared nanocrystals.

4.3. Materials

Paclitaxel (USP, 98-100 %) gift sample was obtained from MSN Laboratories Pvt. Ltd., Unit II, Sy No:50, Kardanur, Medak (Dist.), Telangana, India. Fucoidan (*Undaria pinnatifida*) of medicine grade (98 % fucoidan) was gifted by Nutra Green Biotechnology, Co., Ltd. Shanghai Lvshang Biotechnology, Shanghai-200129, China. Vitamin E TPGS NF Grade was obtained as a gift sample from Antares Health Products, St. Charles, USA. Gift sample of soybean lecithin (SLec.) was received from Lipoid, GmBH. Cholesterol extrapure AR, 99 % (Chol) and Stearylamine AR, 99 % were purchased from SRL chemicals, India. All the solvents used in the experiments were of HPLC grade.

4.4. Methods

4.4.1. Preparation of Polysaccharide Fucoidan based Paclitaxel Nanocrystals

Paclitaxel nanocrystals (FPNCs) were prepared by antisolvent crystallization followed by probe sonication method. Fucoidan (1 % w/v) was used as dispersion stabilizer maintained at a lower temperature (about 2-8 ℃) in ice-cold water and continuous stirring at 4000 rpm. Briefly, 1 mL of PTX ethanolic solution (10 mg/mL) was added drop-by-drop to 10 mL of fucoidan solution (1% w/v) using a 2 mL insulin syringe. Resultant dispersion was probe sonicated for 10 min at amplitude of 50 % and pulse cycle of 07/03 as ON/OFF while maintaining dispersion on ice-cold water. FPNCs were centrifuged for 10 min at -4 °C and 15000 rpm using a high-speed cooling centrifuge, resuspended in 5 mL water for washing and removal of excess polymer. Centrifugation-resuspension-centrifugation was continued for three cycles. At the end, the sediment of FPNCs was resuspended in 5 mL distilled water and lyophilized for further use.

4.4.2. Preparation of Lipid Coated Paclitaxel Nanocrystals (Lipo-NCs)

Lipo-Nanocrystals were prepared using thin film hydration followed ultrasonic dispersion technique. Here, the primary lipid materials were SLec and Chol, while TPGS was employed to increase Lipo-NCs stability, and stearlyamine assisted lipid coating on negatively charged FPNCs (He et al., 2023a). For this, a thin film of 6 mg SLec, 3 mg of Chol, 1 mg TPGS and 1 mg stearylamine was prepared by thin film solvent evaporation method. Then, thin film was rehydrated with 5 mL water containing 10 mg FPNCs, under sonication for 15 min to yield Lipo-NCs. Resultant Lipo-NCs were kept under continuous stirring on ice cold water, Centrifugation-resuspension-centrifugation was done for three cycles, and sediment of Lipo-NCs was collected by resuspending in 5 mL water, lyophilized for further use.

4.4.3. Characterization of Nanocrystals

4.4.3.1. *Particle Analysis: Size, Polydispersity Index (PDI), Zeta Potential, Encapsulation Efficiency and Drug Loading*

Particle size, PDI and zeta potential of FPNCs and Lipo-NCs were determined by photon correlation spectroscopy (PCS) using Zetasizer (Nano ZS, Malvern Instruments, Malvern, UK). The encapsulation efficiency (EE) and drug loading of FPNCs and Lipo-NCs were measured using HPLC. A reverse-phase HPLC column (C18) was used. Briefly, 5 mg of lyophilized powder was added to 5 mL of methanol and vortexed for 10 min for stabilizer membrane disruption. The solution was then centrifuged at 12000 rpm for 10 min, supernatant was collected, filtered through 0.20 μm syringe filter and analyzed using HPLC. The flow rate of mobile phase of ACN: Water (60: 40 v/v) was set at 1.0 mL/min. The column effluent was detected with a UV/VIS detector at 229 nm. The calibration curve was linear in the range of 10–100,000 ng/mL with a correlation coefficient of $R^2 = 0.999$.

4.4.3.2. *Robustness to Dilution and Storage Stability*

Robustness to dilution was also checked to determine the effect of dilution on nanocrystal size. For this, 1 mg/mL nanocrystals were diluted 10, 20, and 50-fold, bath sonicated for 30 sec to disperse the particle homogeneously and the particle size was measured using Zetasizer (Deng et al., 2010). The storage stability for dry powder of FPNCs and Lipo-NCs was investigated at 4 °C and -20 °C ± 4 °C, respectively. At specified time points, particle size, zeta potential, and distribution of nanocrystals (PDI) were measured for determining nanocrystals stability.

4.4.3.3. *Microscopic Measurements*

The morphology and size were determined using scanning electron microscope (SEM, Nova Nano SEM 450, FEI, USA). For sample preparation, the formulation was diluted 20-folds with distilled water, dropped onto the glass slides, and then vacuum dried

overnight at 25 °C. The slide was then gold coated using sputter coater (DSR1) for 120 sec. The surface characteristics like smoothness, and grain distribution was done by scanning probe microscope (SPM, NTEGRA Prima, NT-MDT Service and Logistics Ltd). Sample was prepared similar to SEM except gold coating. The measurements were done using SPM image analysis software (Nova Powerscript 3.4.0 rev 16681).

4.4.3.4. *Solid State Characterization*

Characterization of solid powders of FPNCs and Lipo-NCs was also done using various spectroscopic techniques including Fourier-transform infrared (FT-IR), powder X-ray diffraction (XRD), differential scanning calorimetry (DSC), X-ray photoelectron spectroscopy (XPS), circular dichroism (CD), Solid state ^{13}C NMR and Brunner-Emmett-Teller (BET).

The FTIR study was conducted using SHIMADZU 8400S, Tokyo, Japan. For this, pure PTX, FPPM (1:1 physical mixture of pure PTX and fucoidan), FPNC and Lipo-NCs powder were mixed with KBr in 1:5, pressed into pellets using a hydraulic press and recorded between 4000 cm^{-1} to 600 cm^{-1} at a resolution of 4 cm^{-1} and a scan rate of 64 accumulation per min.

The XRD study was conducted to determine the conversion of crystalline drug to nanocrystals (FPNC) and lipid coated crystals (Lipo-NCs) of amorphous nature. XRD was conducted using Rigaku Miniflex 600 powder x-ray diffractometer equipped with a D/teX Ultra detector. The diffraction pattern was recorded at a scan rate of 5^{o} min^{-1} over the 2θ range of 5 to 50^{o} and step size of 0.02^{o}.

The DSC study was conducted using Shimadzu DSC-60 Plus between the temperature range of -25 to 300 °C at a heating rate of 20 °C/min and nitrogen purging at 40 mL/min. The XPS was used to assess the surface chemistry of pure PTX, FPNC, and

Lipo-NCs. The solid powder was pressed to form pellets and analysed using K-Alpha model (Thermo Fisher Scientific) with Mg Kα radiation (hν = 1253.6 eV) to obtain the spectra in the range of 100-700 eV binding energy.

Solid state ^{13}C NMR data was collected for pure PTX, fucoidan and FPNC using Advance Neo 600 MHz NMR Spectrometer, Bruker India Scientific. Effective surface area and adsorption desorption Brunauer-Emmett-Teller (BET) surface area analysis of pure PTX and FPNC was also conducted by nitrogen adsorption method at 77.36 K using BELLSORP MAX II & BELCAT-II, Microtrac BEL Corp. To study the drug interaction with excipients, Circular Dichroism Spectrophotometer (CD Polarimeter J-1500, JASCO) was used to check the change in specific conformation of pure PTX on formulation as FPNC and Lipo-NCs.

4.4.3.5. *Water Contact Angle*

The water contact angle of nanocrystals was conducted to determine the wettability of nanocrystals compared to coarse drugs. The study was performed by static contact angle measurement instrument (KRUSS GmbH Germany, DSA 10). For this, lyophilized nanocrystals and the crude drug were punched into tablets (100 mg, pressure 5 kg). For measurement, a drop of simulated lung fluid (~4 µL) was dropped on the plane surface of the tablet through a microinjector, and the camera captured the image. The contact angle values were noted, and measurement was done in triplicate (Jiang et al., 2012).

4.4.3.6. *Saturation Solubility*

The equilibrium solubility of PTX, FPNCs and Lipo-NCs in simulated lung fluid (SLF) was determined using saturation shake-flask method (Kumar et al., 2019d). SLF consisted of 0.02 % w/v DPPC, maintained at 35 °C (Williams et al., 2008). For this, an excess amount of sample was added to SLF shaken at 25 °C in a water-bath shaker

for 48 h and further kept aside for 24 h to achieve equilibrium. The equilibrated liquid was centrifuged for 15 min at 12000 rpm and filtered through 0.2 μm syringe filter (AXIVA) to remove the surplus insoluble excipients. The filtrate was analysed by HPLC at 229 nm using HPLC.

4.4.4. In-Vitro Studies

4.4.4.1. *In-Vitro Drug Release in Simulated Lung Fluid*

The modified dialysis bag diffusion technique was used for studying the in-vitro drug release from FPNCs and Lipo-NCs. For this, 50 mL falcon tube with an open upper end and a lower end assembled with dialysis bag (12 kD) was used. FPNCs and Lipo-NCs equivalent to 5 mg of PTX redispersed in 2 mL SLF was added to the inside of falcon tube (donor compartment) immersed in 48 mL of SLF (acceptor compartment) in a beaker. The entire system was maintained at 37 ± 0.5 °C under continuous stirring at 100 rpm / min. At predetermined time intervals, aliquots of 2 mL were collected from acceptor compartment and replaced with same volume of fresh medium. PTX has poor aqueous solubility and thus 0.1 % (w/v) Tween 80 was included in the release medium to maintain the sink condition for release study. The samples were filtered through 0.20 μm syringe filter prior to drug quantification by HPLC.

4.4.4.2. *Mucus Diffusion*

The ability of nanocrystals to diffuse across the respiratory mucus layer was assessed using a vertical Franz cell apparatus. In this experiment, 0.5 % hydroxyethylcellulose (HEC) solution was used as simulated mucus due to its chemical and microrheological similarities to mucins. Briefly, a pair of polycarbonate filters (Merck Millipore, 2 μm) as diffusion membrane was fixed to the Franz cell, and the gap between the filters was filled with 20 μL 0.5 % hydroxyethylcellulose solution. The effective diffusion area of this setup was 1 cm^2. The acceptor compartment was filled with 7.5 mL phosphate

buffer containing 0.2 % sodium dodecylsulfate solution, and the experiment started by adding 1 mL FPNCs and Lipo-NCs (equivalent to 1 mg PTX) into the donor compartments. The device was maintained at 37 °C with a circulating water bath. After 1 and 6 h of diffusion, sample was collected from the acceptor chamber. The sample was centrifuge at 15000 rpm for 10 min at -4 °C to collect the nanocrystals permeated across diffusion membrane. The sediment was redispersed in distilled water and analyzed for possible intact nanocrystals using Zetasizer. The supernatant collected and sediment reconstituted were used for determining amount of drug diffused across membrane, using HPLC method (He et al., 2020b; Khan et al., 2021).

4.4.4.3. *Powder Flow*

The flowability of pure PTX and fabricated nanocrystals as DPIs was determined using angle of repose method in General Chapter <1174> Powder flow in United States Pharmacopeia (USP). In brief, the powder was poured from a hight through a conical flask to form a static heap of powder as a conical mound. The sides of conical mound make an angle with horizontal surface known as the cone angle of repose. High angle of repose reflects cohesive powder while low angle is for non-cohesive powder (Zendehdel et al., 2022).

4.4.4.4. *Aerosolization Performance*

The aerosolization performance of PTX, FPNCs and Lipo-NCs were determined using eight-stage Anderson cascade impactor (ACI, Westech Instruments, UK) recommended by the Ph. Eur. 6th edition for aerodynamic analysis. The powder (20 mg) was filled in size 3 HPMC capsule (C) and loaded in the device (Rotahaler® Cipla, a commercially available single-dose capsule-based DPI). The inhaler device (D) was connected to the ACI using a mouthpiece adaptor (MP). The capsule was pierced into device prior to actuation in ACI. The test was carried out at a flow rate of 60 L/min and actuation time

of 4 sec. Ten capsules were used in each run for each sample. Post aerosolization, the inhaler device, mouthpiece, induction port (I), pre-separator (PS) and all stages (Table 4.1) were washed using methanol and quantitatively determined by HPLC. Emitted dose (ED) was also determined from particles distributed at each stage of ACI and was the difference between the amount of powder filled into and the amount of powder remaining in the capsule within the DPI device. Fine particle fraction (FPF) was calculated as percentage of drug particles less than 5 μm, deposited at stages 2-7 of ACI. FPF is indicative of particles fraction that are suitable for effective inhalation and assumed to deposit in the lungs to induce a pharmacological effect (Chvatal et al., 2017).

Table 4.1 Effective cut-off diameter of each stage of impactor.

Stage Number	**Stage 0**	**Stage 1**	**Stage 2**	**Stage 3**	**Stage 4**	**Stage 5**	**Stage 6**	**Stage 7**
Cut-off Diameter (μm)	8.6	6.5	4.4	3.2	1.9	1.2	0.6	0.3

4.4.5. In-Vivo Study

Male Wistar rats (body weight 200 ± 20 g) were divided randomly into four treatment groups as Group 1 for *i.v.* administration of pure PTX, while Group 2, 3 and 4 for intra-tracheal administration of pure PTX, FPNC and Lipo-NCs, respectively. Group 5 was untreated group (n=3) for zero time point. The protocol was approved by Institutional Animal Ethical Committee (IIT(BHU)/IAEC/2023/018). Rats were fasted for 12 h prior to the study with water ad libitum, anesthetized by intraperitoneal injection of a mixture of ketamine (80 mg/kg body weight) and xylazine (8 mg/kg body weight) and then equivalent amount (10 mg/kg) of plain PTX, FPNC and Lipo-NCs were intratracheally

administered using 20 G cannula tube and 1 mL syringe (Chaurasiya et al., 2018). After intratracheal dosing, the animals were held in an upright position for 2 min to ensure deposition of dose following the removal of delivery device. For intravenous administration (tail vein injection), free PTX solution was prepared by dissolving pure PTX in 2 mL of Cremophor EL / dehydrated ethanol mixed solution (1:1). The drug solution was bath sonicated for about 30 min and diluted with appropriate volume of PBS (pH 7.4) prior to use (Lin et al., 2014).

For pharmacokinetic and biodistribution studies, the Wistar rats were randomly divided into four treatment groups (n = 18 in each group). Following the treatments, blood samples (0.5 mL) were taken from orbital vein in heparinized tubes at the predetermined time points of 0.5, 1, 3, 6, 12, and 24 h. Blood samples were centrifuged at 6000 rpm for 10 min to isolate the plasma, kept at -80 °C until HPLC analysis was performed. For biodistribution study, three animals from each group at each time point (0.5, 1, 3, 6, 12, and 24 h) were sacrificed and all major organs including liver, lung, kidney, spleen and heart, were removed, rinsed twice with normal saline (0.9 % w/v), and wiped with a filter paper and stored at –20 °C until extraction procedure. To determine PTX concentration in organ samples, organ was homogenized with 80 % aqueous acetonitrile at a ratio of 1:3 (w/v). The tissue homogenates were then centrifuged at 6000 rpm for 10 min and supernatant (organic layer) was collected. The sample was transferred to glass test tubes, dried under vacuum conditions to evaporate the organic layer and re-dissolved in 50 µl of methanol and vortex-mixed with 100 µL of internal standard (docetaxel) solution (100 ng/mL of PTX in ACN). After centrifuging at 12,000 rpm for 10 min, 20 µL of sample was analysed using HPLC (He et al., 2020b). Before that, calibration curves in acetonitrile and plasma or tissue homogenate fraction were prepared and validated. The plasma PTX concentration time

profile was plotted to determine the standard pharmacokinetic parameters using non-compartmental model.

4.5. Statistics

Data were reported as Mean ± SD (n = 3) and statistical analysis were performed using software GraphPad Prism 9.0.0 (GraphPad Software, San Diego, CA, USA). For in-vivo studies, one-way and two-way analysis of variance (ANOVA) was used for determination of statistical significance among multiple groups. Two-tailed student t-test was performed for comparison of two groups. The statistical significance p value was denoted as "****" for $p < 0.0001$, "***" for $0.001 < p > 0.0001$, "**" for $0.01 < p > 0.001$, "*" for $0.05 < p > 0.01$ and "ns" for non-significant.

4.6. Results and Discussion

4.6.1. Characterization of Nanocrystals

The solid-state nanocrystals were successfully prepared as dry powder for inhalation. The nanocrystals were characterized for size, shape, surface chemistry, elemental composition, flowability, and rigidity that were known as "critical nanoscale design parameters" for regulating pharmacokinetics and pharmacodynamics of drug post pulmonary delivery. The nanocrystals were rod shaped particles with smooth morphology. The size and zeta potential of FPNC was 350 ± 54 nm and -37 ± 2.74 mV, respectively. The negative charge on FPNC was due to anionic fucoidan on crystals surface. The size of Lipo-NCs was about 900 ± 21 nm which was higher than FPNC. The increase in size was probably due to surface coating of FPNC with lipid layer. The zeta potential of Lipo-NCs was found to be 19 ± 4.23 mV due to coating of anionic fucoidan with positively charge lipid layer (He et al., 2023a). FPNC and Lipo-NCs had a polydispersity index of < 0.3 and thus were homogeneously dispersed. The shape and morphology of nanocrystals was determined by SEM and AFM (Figure 4.1). SEM

revealed a rod shape for FPNC of about 360 nm with blunt edges. In addition, the Lipo-NCs were broader and rod shaped of about 950 nm with round edges. The AFM images of FPNC and Lipo-NCs also showed smooth surface particles of about 400 nm and 1000 nm, respectively, and the results were in agreement to SEM. FPNC and Lipo-NCs exhibited an entrapment efficiency of 84.60 ± 4.53 % and 73.58 ± 3.17 %, respectively. While, drug content was 65 ± 0.42 % for FPNC and 54 ± 1.30 % for Lipo-NCs.

Figure 4.1 A & D) SEM images; B & E) AFM images and C & F) TEM images of FPNC and Lipo-NCs, respectively.

Prepared nanocrystals were robust to dilution and highly stable during storage, showing non-significant change in particle size, zeta potential and PDI (Figure 4.2 & 4.3).

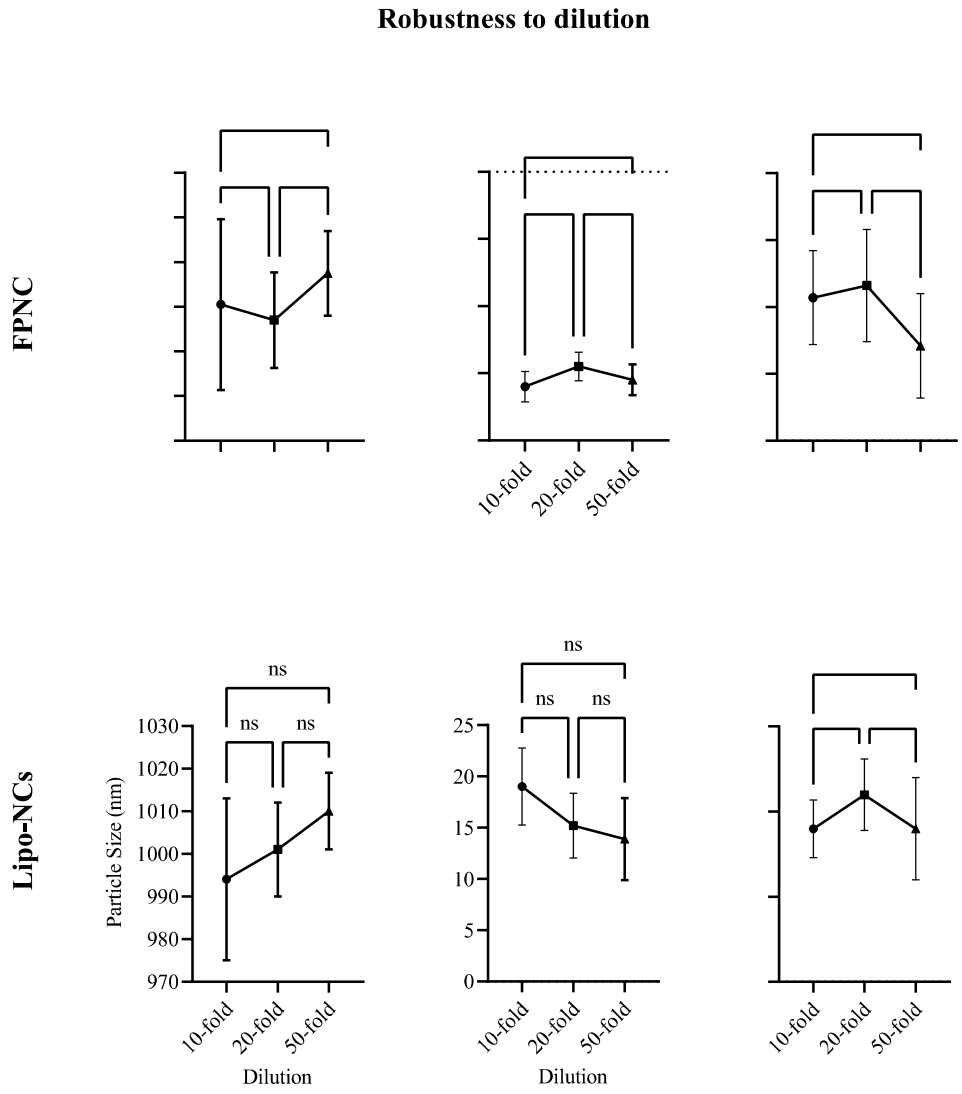

Figure 4.2 Robustness of prepared nanocrystals (FPNC and Lipo-NCs) to dilutions at different folds. The data were presented as mean ± standard deviation (n=3). One-way ANOVA was used for comparing groups using Turkey's multiple comparison test at significance of p< 0.05; "ns" denoted non-significant difference.

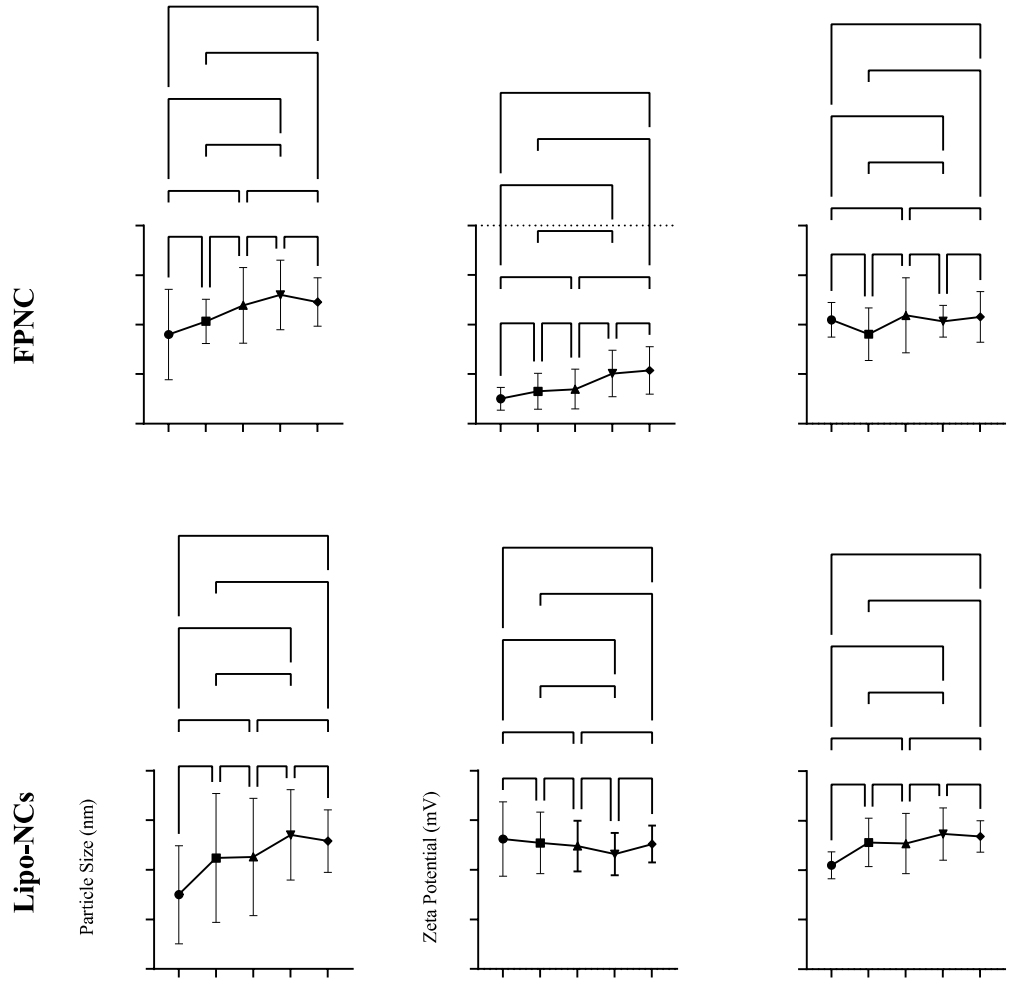

Figure 4.3 Storage stability study of FPNC and Lipo-NCs for changes in particle size, PDI and zeta potential. The data were presented as mean ± standard deviation (n=3). One-way ANOVA was used for comparison between groups using Turkey's multiple comparison test at p< 0.05; "ns" denoted non-significant difference.

The FTIR spectra of PTX, FPPM, FPNC, and Lipo-NCs were shown in Figure 4.4. The characteristic absorption peaks for crystalline PTX were observed at 1734.50 cm^{-1} (C=O stretching vibration), 1707.39 cm^{-1} (C=O stretching vibration of ester group), 1645.71 cm^{-1} (N=H bond), 1246.43 cm^{-1} (C-N stretching) and 706.65 cm^{-1} (C–C

stretching). Peaks observed were as reported previously for pure PTX (Sakhi et al., 2022; Zhou et al., 2017). Physical mixture also showed absorption peaks similar to PTX at 1738.23 cm^{-1}, 1707.90 cm^{-1}, 1645.48 cm^{-1}, 1244.37 cm^{-1} and 706.65 cm^{-1}.

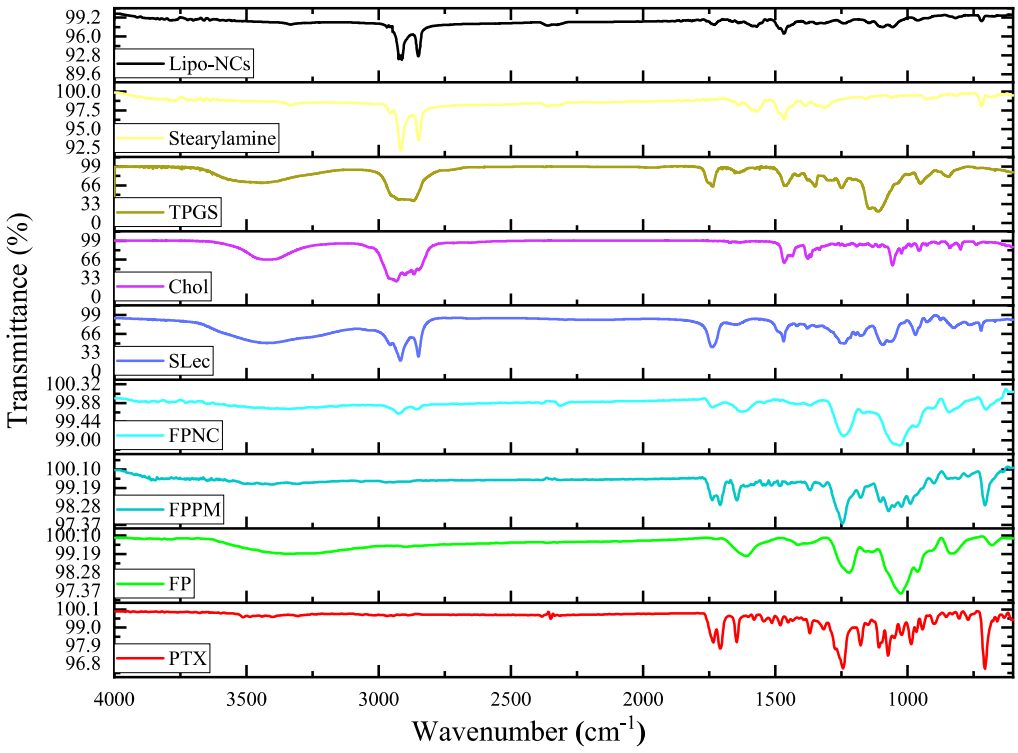

Figure 4.4 FTIR Spectrum of pure PTX, fucoidan (FP), physical mixture of drug and polymer in 1:1 (FPPM), FPNC, Soy-lecithin (SLec), cholesterol (Chol), TPGS, stearylamine, and Lipo-NCs.

However, the peak intensity decreased due to dispersion of PTX in polymer on physical mixing that resulted in partial coating of PTX. In contrast, the characteristic peaks of PTX were absent in FPNC with very low intensity peak band at 1736.64 cm^{-1}, 1622.11 cm^{-1}, 1242.13 cm^{-1}, and 700.62 cm^{-1}. This could be due to the presence of fucoidan on the surface drug nanocrystals that masked the peaks of pure drug. Furthermore, Lipid coating on fucoidan stabilized nanocrystals was done using SLec, Chol, and stearylamine. Lipo-NC did not exhibit peaks of PTX suggesting that drug was not

leached out during the process of coating due to which characteristic peaks of pure drug. The trend followed by Lipo-NCs was different from FPNC and was merged of lipid mixture attributed to lipid layer coating on surface of FPNC. The spectrum of Lipo-NCs showed peaks at 1728.03 cm^{-1} and 719.58 cm^{-1} corresponding to SLec (C=O stretching vibration) (Wang et al., 2014) and stearylamine (NH2 wagging vibration) (Sabry et al., 2021; Witoonsaridsilp et al., 2012; Zidan et al., 2010).

XRD spectrum of PTX, FPNC and Lipo-NCs is represented in Figure 4.5. Diffraction pattern of PTX showed characteristic peaks at 2θ of 5.712˚, 9.0156˚, 10.126˚, 11.346˚, 12.531˚, 14.011˚, 14.756˚, 15.750˚, 17.180˚, 18.067˚, 18.843˚, 19.85˚, 21.141˚, 22.085˚, 22.911˚, 25.331˚, 27.269˚, 28.782˚ and 30.057˚. Similar peaks were observed for pure PTX at 2θ of 5.4˚, 9˚, 10˚, 11.2˚, 12.55˚ and 13.55˚ (Wu et al., 2022; Zhou et al., 2017). Physical mixture (FPPM) of fucoidan and PTX exhibited peaks at 5.950˚, 9.288˚, 10.419˚, 11.586˚, 12.772˚, 15.308˚, 15.982˚, 17.444˚, 19.091˚, 19.989˚, 21.104˚, 22.319˚, 25.555˚, 27.512˚, 29.023˚ and 30.279˚. The diffraction pattern of physical mixture was similar to coarse drug along with amorphous pattern of polymer, however the peaks observed were of decreased intensity. This could be due to partial coating of crystalline PTX with fucoidan on physical mixing and lack of co-solvation and co-precipitation (Deng et al., 2010). PTX nanocrystals (FPNC) had peaks at 6.022˚, 9.618˚, 10.790˚, 12.420˚, 13.731˚, 15.303˚, 16.362˚, 18.755˚, 20.263˚, 21.136˚, 22.107˚, 23.952˚, 26.356˚, 28.821˚ and 30.696˚. In addition, the peaks were of very low intensity and slightly shifted to right (higher 2-theta), that could be due to encapsulation of drug in fucoidan and formation of reduced size particles. The major peaks for Lipo-NCs were at 5.257˚, 6.128˚, 8.461˚, 9.662˚, 10.874˚, 12.490˚, 14.032˚, 16.443˚, 18.858˚, 20.312˚, 22.198˚, 24.079˚, and 26.431˚, corresponding to diffraction pattern of lipid

composition. The big broad peak at 21.170˚ was due to amorphous SLec (Wang et al., 2014), suggesting successful coating of SLec on surface of nanocrystals.

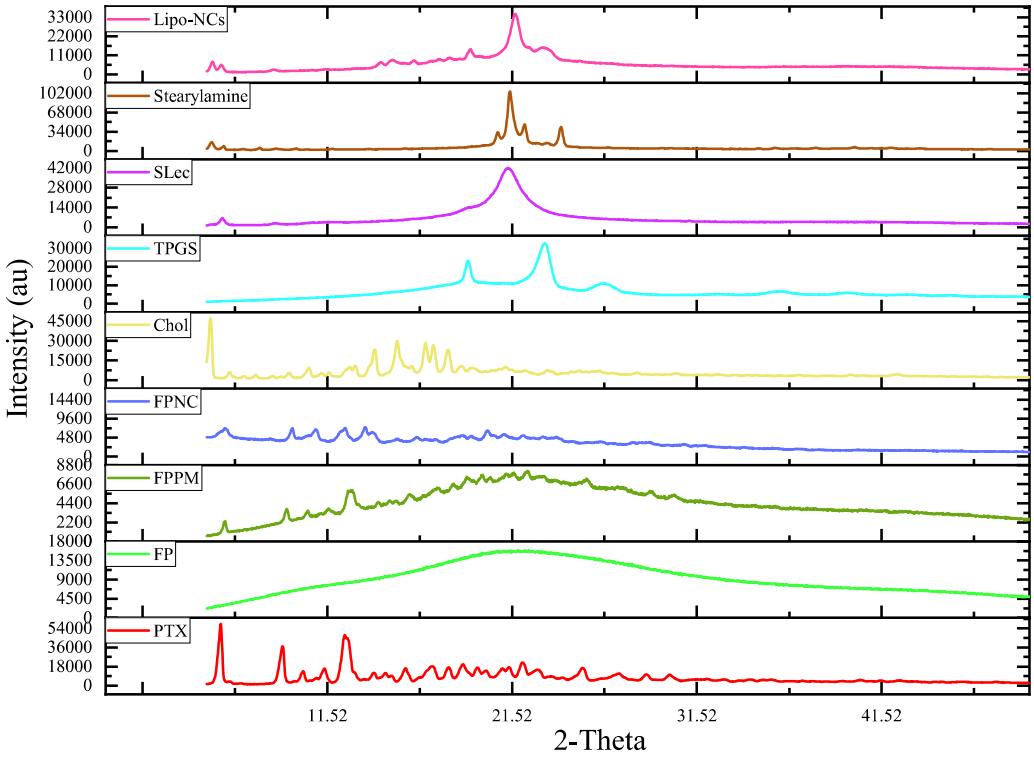

Figure 4.5 XRD Diffraction pattern of pure PTX, fucoidan (FP), physical mixture of drug and polymer in 1:1 (FPPM), FPNC, Soy-lecithin (SLec), cholesterol (Chol), TPGS, stearylamine, and Lipo-NCs.

DSC thermogram of pure PTX showed an endothermic peak at 224 °C corresponding to its melting point and indicated crystalline nature (de Sousa Marcial et al., 2017). The physical mixture showed a remarkably lower endothermic peak at 219 °C that could be due to interaction of drug with polymer (Figure 4.6). FPNC showed absence of endothermic peak of PTX that could be due to encapsulation of drug in polymer network, resulting in conversion of crystalline drug to an amorphous or molecularly dispersed state (de Sousa Marcial et al., 2017). In addition, Lipo-NCs exhibited distinct peaks at 36 °C, 69 °C, 112 °C and 265 °C attributed to lipid coating (TPGS, stearylamine, and SLec).

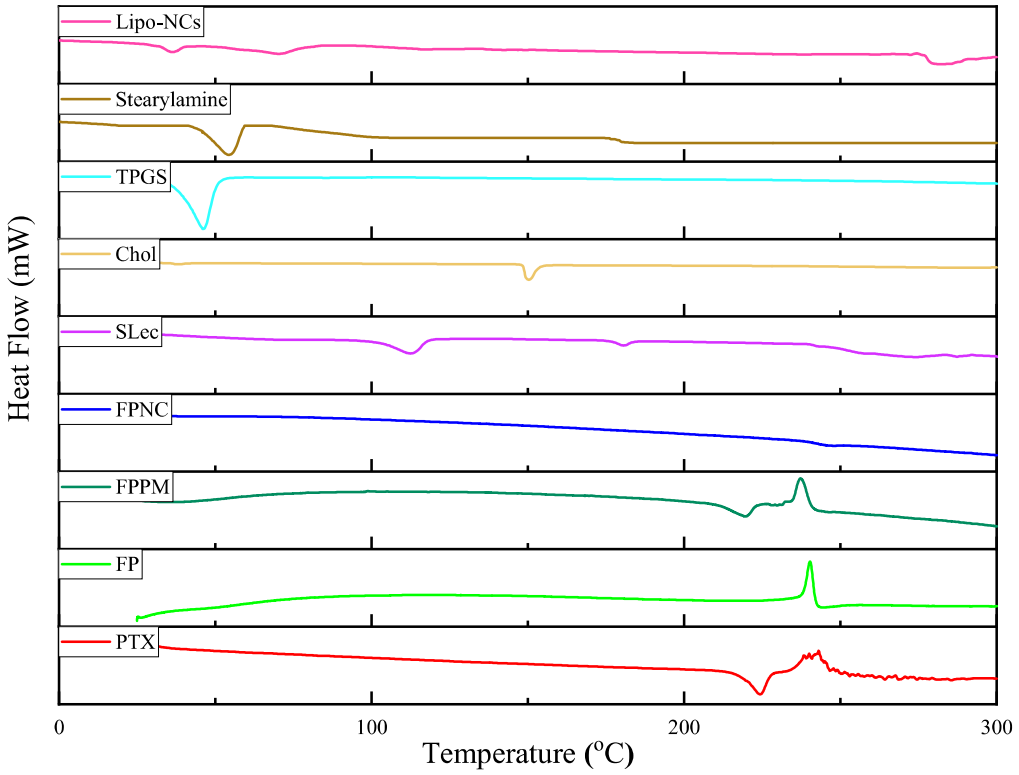

Figure 4.6 DSC thermogram of pure PTX, fucoidan (FP), physical mixture of drug and polymer in 1:1 (FPPM), FPNC, Soy-lecithin (SLec), cholesterol (Chol), TPGS, stearylamine, and Lipo-NCs.

The XPS spectra of PTX, FPNC and Lipo-NCs showed signature C1s, N1s, O1s and S2p peaks (Figure 4.7 A). The atomic percentages of C1s, O1s, and N1s in PTX were 73.10 %, 11.31 %, and 10.93 %, respectively. For FPNC, the atomic percentages of C1s, O1s, N1s and S2p were observed as 73.16 %, 11.58 %, 9.78 % and 0.92 %, respectively. Decrease in N1s percentage was due to molecular dispersion of PTX in fucoidan core while S2p percentage was due to polymer fucoidan. Lipo-NCs exhibited higher atomic percentages of C1s (83.42 %) and O1s (12.26 %) and a lower N1s percentage of 4.09 %. In addition, the S2p was absent and P2p was present in Lipo-NCs XPS. This was due to surface coating of FPNC with lipid layer.

Figure 4.7 A) XPS and B) CD spectrum of pure PTX, FPNC and Lipo-NCs.

CD spectroscopy can be used to undertake the conformational analysis of PTX with a chiral core (Izumi et al., 2008). It can help in investigating the effects of composition on incorporation of paclitaxel in lipo-NCs (Campbell et al., 2001). The CD spectrum of soluble paclitaxel (in ethanol) showed prominent band at 298 nm and a small band of triple intensity at 264 nm (Figure 4.7 B). A multiple band region between and 250-200 nm was also observed for PTX. For soluble paclitaxel, the ellipticity of the positive band at 232 nm is twice that of the negative band at 298 nm (Campbell et al., 2001). The CD spectra of FPNC and Lip-NCs changed, showing aa high intensity band at around 300 nm, similar to previously reported for PTX loaded HSA and hyaluronidase NPs (Kim et al., 2021). The results provided strong evidence of physical interaction between drug and polymer or lipid composition, responsible for masking of characteristic band of PTX.

Nanoparticles are not usually amenable to study by solution-state NMR due to their sub-micron size, since their slow molecular tumbling leads to short nuclear T_2 relaxation times and broader lines. In addition, Nanoparticle samples were amorphous and may have a polydispersity of particle sizes in a given sample. In regard to this, solid-state NMR (ssNMR) spectroscopy emerged as a powerful technique to probe molecular structure of nanoparticles, since it is one of the few techniques capable of providing information of amorphous solid materials. Solid state NMR spectra of coarse drug and nanocrystals is shown in Figure 4.8. The solid-state NMR spectral pattern reflects the anisotropic motion of solid crystalline paclitaxel, and reveals structural information beyond that available from the solution spectrum. In particular, the double ^{13}C peak pattern in solid state indicated a rigid crystalline packing for paclitaxel. The carbonyl C_2 resonance (203.57 ppm) split up into two major peaks (202.39 and 200.57 ppm), indicating a non-equivalent molecular environment in the unit cell or conformational effects in a rigid crystal packed molecule. The reported X-ray crystal structure of PTX has two molecules per unit cell with different C-13 side-chain conformations and peak splitting observed here can be attributed to non-equivalence of two conformations in the crystalline PTX (Chen et al., 2005). In contrast to crystalline PTX, spectral intensity and resolution of peaks were dramatically decreased in FPNC due to molecular dispersion of PTX in fucoidan and lower mobility of molecules (Chen et al., 2005). The NMR spectra of both forms were different reflecting the substantial change in structure of PTX and FPNC. Table 4.2 lists the chemical shifts for crystalline drug and nanocrystals. A low intensity signal, broadened and slightly shifted were observed for drug nanocrystals compared to crystalline drug (Skotnicki and Hodgkinson, 2022). This could be due to intermolecular interaction (non-bonding or physical) of crystalline drug with amorphous polymer used as

stabilizer that resulted in change in local mobility of drug (Budiman and Aulifa, 2022; Chen et al., 2005). Compared to the crystalline drug, ^{13}C peaks of nanocrystals were much broader and of lower intensity, which is mainly attributed to disordered molecular packing (F. Yang et al., 2016). The resonances reflected multiple significantly different environments and a dispersion of chemical shifts similar to disordered materials or amorphous particles (Lubach and Hau, 2018). This suggested the conversion of crystalline drug into amorphous particles.

Table 4.2 Solution and Solid-state ^{13}C NMR chemical shifts of pure PTX and FPNC.

Carbons	Solution NMR	^{13}C Solid-state CP/MAS NMR		
	PTX ^{13}C (ppm)	PTX ^{13}C (ppm)	FPNC ^{13}C (ppm)	FP ^{13}C (ppm)
C-2	203.64	202.39 200.57	205.49 200.17	
C-33	172.73	170.02	170.54	173.31
C-22	171.26	168.38	169.55	
C-30	170.38	167.80 167.25	168.23 167.06	
C-54	167.02	162.44		
C-39	167.07	164.59 163.73	164.21	
C-14	141.98	140.73	140.32	
C-40	137.99	138.75	138.08	
C-37	133.73	136.42		
C-59	133.22	133.16		
C-8	133.65	134.50	134.33	
C-49	131.99	131.85	131.61	
C-56	130.22	131.09	130.17	
C-57, 61	129.18	129.88		
C-58, 60	129.05	129.14		

Carbons	Solution NMR	^{13}C Solid-state CP/MAS NMR		
	PTX ^{13}C (ppm)	PTX ^{13}C (ppm)	FPNC ^{13}C (ppm)	FP ^{13}C (ppm)
	128.74 [C-45, 43, 48, 50] 128.71 [C-47, 51] 128.39 [C-C42, 46] 127.50 [C-44]	127.24 126.35 125.65	126.87 125.80 124.27	98.64 91.21
C-11	84.42	82.77 81.66	81.57	
C-12	81.18	80.98		
C-6	79.06	79.44		
C-1	77.27 77.02 76.76	77.15	77.43	
C-20	76.52	76.11	76.59	
C-5	75.58	75.60	75.90	
C-35	74.97	73.79	73.38	
C-9	73.21	72.87 72.19	72.43 71.71	72.45
C-15	72.40 72.20	70.43	70.41	69.48
		69.78 69.03 68.18 66.31	69.72 69.11 67.99 66.23	66.94 64.10 59.30
C-3	58.64	56.28		
C-36	55.05	55.18	55.50	
			54.28	
C-4	45.64	52.46		
C-7	43.19	44.49	43.85	
C-10	35.71	40.53	40.71 40.02	40.6
C-13	35.63	35.10	35.15	
C-63	26.88	33.94 33.10 31.78	34.64 31.94 30.66	

Carbons	**Solution NMR**	**^{13}C Solid-state CP/MAS NMR**		
	PTX ^{13}C (ppm)	PTX ^{13}C (ppm)	FPNC ^{13}C (ppm)	FP ^{13}C (ppm)
		24.11	24.08	
C-23	22.64	22.87	22.52	
		21.19	21.12	
C-64	21.83	19.76	19.48	
C-31	20.85	18.45	18.59	18.49
C-16	14.85	17.32		
C-28	9.57	10.81 9.89	10.81 9.66	

Figure 4.8 13C solid-state NMR spectrum of FP, pure PTX and FPNC.

Solubility improvement for hydrophobic drugs is extremely important for DPI as hydrophobic particles get rapidly cleared by mucociliary action, macrophage uptake or translocation from the lungs to lymphatic system. In contrast, hydrophilic particles can exhibit faster dissolution in lung thereby avoiding premature clearance. Thus, drug solubility can be improved by increasing the effective surface area or converting hydrophobic drug to hydrophilic particles. The BET study was conducted to confirm

the increase in effective surface area as a result of PTX fabrication as nanocrystals. Pure PTX exhibited a surface area of about 2 $m^2 g^{-1}$. In contrast to this, nanocrystals had significantly increased surface area of about 25 $m^2 g^{-1}$ as measured by BET analysis (Figure 4.9). In addition, gas adsorption also increased to about 250 $cm^3 g^{-1}$ compared to pure drug with a low nitrogen adsorption capacity of only 25 $cm^3 g^{-1}$. This suggested the higher effective surface area of nanocrystals compared to pure PTX.

Figure 4.9 BET analysis of pure PTX and FPNC; A & B) effective surface area of PTX and FPNC, respectively; C & D) nitrogen adsoption potential of PTX and FPNC based on their effective surface area.

The hydrophilicity of particle can be determined from wettability study to estimate their affinity towards aqueous media (Figure 4.10). The results revealed a lower contact angle for FPNC (about 20˚) compared to pure PTX (82˚). Lower contact angle attributed to hydrophilic fucoidan used for nanocrystal fabrication that improved the wettability of hydrophobic PTX (Jiang et al., 2012). The study thus confirmed the conversion of the hydrophobic PTX to a hydrophilic amorphous form. In addition, Lipo-NCs had a higher contact angle of about 38˚ compared to FPNC. The higher

contact angle could be due to lipid coating over surface of nanocrystals. However, the contact angle was still low than pure PTX.

Figure 4.10 Water contact angle of pure PTX (A) FPNC (B) and Lipo-NCs (C).

The saturation solubility study further confirmed the role of increased effective surface area and wettability in increasing the drug solubility in lung fluid (Figure 4.11 A). FPNC and Lipo-NCs exhibited the saturation solubility of about 3.29 ± 0.011 μg mL^{-1} and 2.65 ± 0.52 μg mL^{-1}, respectively while pure PTX exhibited solubility of only 0.347 ± 0.047 μg mL^{-1}. Fabricated nanocrystals improved the solubility by 7-10 folds attributed to lower particle size, increased effective surface area and hydrophilic surface (Sharma et al., 2016). Therefore, fabricated nanocrystals observed to have high effective surface area and hydrophilic surface responsible for high solubility in lung fluid and thus can avoid ciliary and macrophage clearance.

4.6.2. In-Vitro Studies

In-vitro drug release was conducted in simulated lung fluid to estimate the in-vivo behavior of fabricated nanocrystals at target site (Figure 4.11 B). Pure PTX had a very slow drug release rate, releasing only 7 % in 6 h and 15 % in 48 h. For FPNC, drug release rate was significantly improved by many fold (about 57 % in 6 h and 99 % in 48 h) compared to coarse drug. This could be due to reduced particle size and incorporated hydrophilic fucoidan as stabilizer. Higher drug release from nanocrystals suggested

faster systemic absorption, and higher distribution but lower retention in lung. To increase the drug retention in lung, FPNC were coated with lipid layer. In contrast to FPNC, Lipo-NCs had a slower drug release rate (27 % in 6 h and 75 % in 48 h), however the release was significantly higher than pure PTX. Slower drug release from Lipo-NCs was attributed to lipid membrane of TPGS and SLec (He et al., 2023a). This in turn will increase the drug residence in lung and slow down the transport of drug across lung epithelium to systemic circulation, compared to highly soluble FPNC. Additionally, positively charge Lipo-NCs can also interact with anionic respiratory mucus responsible for impeded transport. These features of Lipo-NCs could help in prolonged retention of drug in the lung for localized target action (He et al., 2023a). The release mechanism was also determined by fitting the release profile to various release kinetic models using DDSolver Add-in program (Table 4.3). The PTX followed Fickian diffusion and erosion controlled slow drug release kinetics. The possible three release mechanism that Pure PTX followed were Peppas-Sahlin (0.9939), Gompertz (0.9954) and Makoid-Banakar (0.9933). The release was controlled by Fickian diffusion (concentration gradient dependent) and was observed for drug with intermediate or slow-release rate. The diffusion index n was 0.499 (i.e., $0.45 < n < 0.89$) as observed in Makoid–Banakar model, suggesting drug release due to erosion as well as diffusion (Li et al., 2020b). FPNC exhibited Fickian diffusion, polymer relaxation, erosion-controlled diffusion or combination of erosion and diffusion, following Peppas-Sahlin (0.9901), Weibull (0.9935) and Makoid-Banakar (0.9906) models. Weibull model suggested an immediate drug release for FPNC and the β value of 0.768 (β values in range of 0.75–1.0) was for diffusion mechanism via erosion (Özdal et al., 2022). The diffusion index n was 0.566 ($0.45 < n < 0.89$) in Makoid–Banakar model showing release due to combination of erosion and diffusion (Li et al., 2020b). While,

Lipo-NCs release was dependant on matrix swelling, relaxation processes, diffusion, and erosion, following Peppas-Sahlin (0.9972), Weibull (0.9966) and Makoid-Banakar (0.9973) model. Weibull model also confirmed a controlled drug release via diffusion mechanism with β value of 0.677 (i.e., β values below 0.75) (Özdal et al., 2022). The diffusion index n of 0.584 observed in Makoid–Banakar release model was in range of $0.45 < n < 0.89$, suggested drug release via combination of erosion and diffusion (Li et al., 2020b). Weibull and Makoid-Banakar model were also reported for polymeric nanoparticles (Özdal et al., 2022), PLGA-based nanoparticles (Martín-Camacho et al., 2023), and DPPC coated lipid nanoparticles for pulmonary delivery (Li et al., 2020b).

Table 4.3 Drug release fitted to various release kinetic models.

Release Model	**PTX**	**FPNC**	**Lipo-NCs**
	R^2		
Zero-order (F=k0*t)	0.4275	0.1872	0.7065
First-order	0.4879	0.9781	0.9316
Higuchi	0.9485	0.8643	0.9933
Korsmeyer-Peppas	0.9844	0.9490	0.9937
Hixson-Crowell	0.4681	0.9132	0.8864
Peppas-Sahlin m is 0.43 for a sphere, k1 is Fickian diffusion, k2 relaxation.	0.9939 k1 = 3.205 k2 = -0.166 m = 0.534	0.9901 k1 = 24.373 k2 = -1.486 m = 0.581	0.9972 k1 = 10.434 k2 = -0.316 m = 0.612
Quadratic	0.8420	0.8098	0.9427
Weibull	0.9861	0.9935; α = 4.408 β = 0.768	0.9966 α = 9.989 β = 0.677

Logistic	0.9875	0.9850	0.9907
Gompertz	0.9954 $\alpha = 3.496$ $\beta = 0.371$	0.9703	0.9694
Probit	0.9922	0.9878	0.9874
Hopfenberg	0.4875	0.9781	0.9316
Baker-Lonsdale	0.9557	0.9716	0.9898
Makoid-Banakar	0.9933; n = 0.499	0.9906; n = 0.566	0.9973; n = 0.584

Drug diffusion across mucus was also studied to check the nanocrystals and lipid coating role in facilitating permeation across mucus membrane (Figure 4.11 C). The study showed poor diffusion of pure PTX to about 4.3 µg/mL in 1 h and 10.05 µg/mL in 6 h. In contrast, FPNC significantly improved the drug diffusion to 29.45 µg/mL in 1 h ($p = 0.0001$) and 59 µg/mL in 6 h ($p < 0.0001$). The lipo-NCs had the drug diffusion of 21.35 µg/mL in 1 h and 49.8 µg/mL in 6 h, which was significantly higher to coarse drug ($p = 0.003$ in 1 h and $p < 0.0001$ in 6 h), but lower to FPNC. Lower mucus diffusion of Lipo-NCs than FPNC could be due to interaction of positively charged Lipo-NCs with the mucus layer, resulting in reduced transport and increased lung residence (He et al., 2023a). However, the difference was not significant between FPNC and Lipo-NCs ($p = 0.153$ in 1 h and $p = 0.1056$ in 6 h). The higher mucus diffusion of Lipo-NCs than pure PTX was attributed to its sub-micron size and membrane fluidity due to lipid composition (mainly phospholipid and TPGS). The results were in accordance to in-vitro drug release results and suggested the potential of Lipo-NCs in prolonging drug retention in lung.

Figure 4.11 A) Saturation solubility study in simulated lung fluid; B) In-vitro drug release profile; C) Histogram for drug diffusion across simulated mucus; and D) Angle of repose of PTX, FPNC and Lipo-NCs. Data were shown as mean ± standard deviation (n = 3) and Two-way ANOVA was used for comparison of groups using Turkey's multiple comparisons test at $p < 0.0001$ (****), $p < 0.001$ (***), $p < 0.01$ (**), and non-significant (ns).

Solid powder for inhalation should have good flow property as it plays key role in aerosolization performance of powder. Prepared FPNC and Lipo-NCs exhibited an angle of repose of 27° and 29°, indicative of excellent flow. Whereas, pure PTX showed an angle of repose of 37° reported for fair flow. The angle of repose pf pure PTX was significantly higher than prepared nanocrystals (Figure 4.11 D). Therefore, FPNC and Lipo-NCs had higher flowability suitable for administration as DPIs.

Aerosolization behavior of prepared nanocrystals dry powder was conducted using ACI to determine their capability for pulmonary administration.

Figure 4.12 A) Particle distributed of PTX, FPNC and Lipo-NCs at each stage of ACI. B) Histogram of particle deposited and C) Percentage drug deposited to each part and all stages of Anderson cascade impactor (ACI) assembly. Bar diagrams were shown as mean ± standard deviation (n=3).

As shown in Figure 4.12, the aerosolization performance of FPNC and Lipo-NCs compared to pure PTX. FPNC and Lipo-NCs was higher with higher particle distribution to lower stages of ACI, compared to pure PTX (Figure 4.12 A & B). This could be due to lower particle size and good flow property of prepared dry powder of nanocrystals. The ED for all samples was higher than 90 % suggesting excellent aerodynamic behavior. The FPF value was highest for FPNCs (60.15 %) followed by L-FPNCs (55.70 %) and PTX (39.90 %). FPF value was over 50 % favorable for pulmonary deposition to lung (Chvatal et al., 2017). The nanocrystals resulted in high drug distribution to lower stage of ACI, indicating suitability for drug deposition to deep lung (Figure 4.12 C). Results also suggested superior aerosolization performance for prepared nanocrystals compared to pure PTX. Difference in results could be due to i) homogenous structure of nanocrystals, ii) low aggregation and high dispersion potential under shear forces, attributed to high stability, and iii) unique rod-shape morphology that might facilitated better particle distribution and low inter-particulate interaction (Zhou et al., 2020).

4.6.3. In-Vivo Studies

Pharmacokinetic study was conducted to determine the in-vivo performance of pure PTX, FPNC and Lipo-NCs. Figure 4.13 A showed the pharmacokinetic profile of pure PTX (*i.v.*), pure PTX (inh.), FPNC, and Lipo-NCs. PTX (*i.v.)* had lower MRT of 2.5 h and the plasma concentration also decreased at a faster rate, compared to FPNC and Lipo-NCs. In contrast, FPNC and Lipo-NCs exhibited plasma concentration time profile with slower drug elimination than pure PTX. Higher $t_{1/2}$ and MRT were observed for FPNC and Lipo-NCs compared to pure PTX (inh.) and PTX (*i.v.*). Also, AUC of FPNC and Lipo-NCs was significantly higher ($p < 0.0001$) than pure PTX

(inh.). This suggested transport of drug from lung to systemic circulation over a longer period. C_{max} and AUC of PTX (inh.), FPNC, and Lipo-NCs was significantly lower ($p < 0.0001$) than PTX (*i.v.*). Results revealed lower drug in systemic circulation when administered intratracheally. FPNC and Lipo-NCs were capable of reducing C_{max} and AUC to a lower value so that maximum drug is retained in target organ and less free drug reach systemic circulation, thereby minimizing off target distribution and reducing PTX related adverse effects. In addition, AUC of FPNC and Lipo-NCs was significantly higher ($p < 0.0001$) than pure PTX (inh.) (Table 4.4). Also, the AUC of FPNCs was significantly higher ($p < 0.0001$) than Lipo-NCs. This suggested role of nanocrystals in improving drug absorption. The higher AUC of NCs could be due to high solubility in lung fluid and high permeation potential. Higher $t_{1/2}$ and MRT were also observed for FPNC and Lipo-NCs compared to pure PTX (inh.) and PTX (*i.v.*). The results suggested higher retention of drug when formulated as nanocrystals and administered intratracheally. The higher retention of Lipo-NCs in lung than FPNCs could be due to their larger size, shape, cationic charge and lipid coating that hindered faster dissolution of NCs in lung fluid (Choi et al., 2010).

Biodistribution study further revealed significantly lower drug distribution to lung by PTX (*i.v.*) compared to FPNCs and Lipo-NCs (Figure 4.13 B). The PTX (*i.v.*) treated groups also exhibited higher drug distribution to other organs compared to the intratracheal administered groups indicating non-selective biodistribution of intravenous PTX.

Figure 4.13 A) Plasma-PTX concentration time profile, and B) Histogram for drug distribution in lung by PTX (*i.v.*), PTX (Inh.), FPNC (Inh.) and Lipo-NCs (Inh.). C-F) Histogram for drug distribution in other major organs at different time points by PTX (*i.v.*), FPNC (Inh.) and Lipo-NCs (Inh.). All data were shown as mean ± standard deviation (n = 3) and Two-way ANOVA was used for comparison

of groups using Turkey's multiple comparisons test at $p < 0.0001$ (****), $p < 0.001$ (***), $p < 0.01$ (**), $p < 0.05$ (*), and non-significant (ns).

Table 4.4 Pharmacokinetic parameters for plasma concentration time profile of PTX administered intravenously and intratracheally to the rats.

Parameter	*PTX (*i.v.*)	*PTX (Inh.)	*FPNC (Inh.)	*Lipo-NCs (Inh.)
C_{max} (ng/ml)	16404.79 ± 2116.4	953 ± 51.178	2917.65 ± 374.45	1851.46 ± 116.105
Tmax (h)	-	3	3	6
AUC_{0-t} (ng/ml.h)	39927.18 ± 4515.65	4758.55 ± 431.275	24775.50 ± 2220.30	27249.30 ± 1752.04
$t_{1/2}$ (h)	4.69 ± 0.140	4.95 ± 0.193	7.07 ± 0.128	7.85 ± 0.221
MRT (h)	2.446 ± 0.033	7.353 ± 0.363	10.26 ± 0.241	12.87 ± 0.082

**n=3, mean ± standard deviation.*

PTX administered via inhalation route had significantly lower drug concentration in lung than FPNCs and Lipo-NCs. This lower drug concentration in lung, despite the localized administration may be attributed to the lower dissolution of hydrophobic PTX and the subsequent mucociliary clearance from lung. In contrast, higher lung retention was observed with FPNC and Lipo-NCs as compared to pure PTX. FPNC concentration in lung decreased with time and was significantly lower to Lipo-NCs. However, the concentration was higher compared to pure PTX. Compared to FPNC and pure PTX, drug concentration was significantly higher in lung for Lipo-NCs treated groups, suggesting higher retention of Lipo-NCs in lung over an extended period of time. FPNC and Lipo-NCs also had significantly lower drug distribution to other organs than lung, as compared to pure PTX (Figure 4.13 C-F).

Table 4.5 Pharmacokinetic parameters for lung concentration time profile of PTX administered intravenously and intratracheally administration to the rats.

Parameter	*PTX (*i.v.*)	*PTX (Inh.)	*FPNC (Inh.)	*Lipo-NCs (Inh.)
C_{max} (ng/g)	17450.29 ± 1207.90	76630.67 ± 1207.95	153084.67 ± 7322	158436.60 ± 9331.50
T_{max} (h)	0.5	0.5	0.5	0.5
AUC_{0-t} (ng/g.h)	42765.04 ± 2472.41	302336.50 ± 10728.8	1279123.021 ± 112214	1590926.443 ± 315355
$t_{1/2}$ (h)	5.146 ± 0.076	4.793 ± 0.011	6.831 ± 0.070	11.188 ± 0.081
MRT (h)	4.382 ± 0.034	6.334 ± 0.021	9.363 ± 0.102	16.312 ± 0.013

**n = 3, mean ± standard deviation.*

As shown in Table 4.5, pulmonary administration increased the C_{max} and AUC of drug in lung compared to *i.v.* administration. Additionally, nanocrystals given via inhalation improved the pharmacokinetic parameters of drug showing significantly higher C_{max} ($p < 0.0001$) and AUC ($p < 0.0001$), than pure PTX. The drug concentration in lung was 7, 30, and 37-fold for PTX (inh.), FPNC and Lipid-NCs, respectively compared to PTX (*i.v.*). Also, nanocrystals increased the drug retention in lung, showing maximum MRT for Lipo-NCs followed by FPNC, PTX (Inh.) and PTX (*i.v.*). Compared to FPNC, Lipo-NCs had higher $t_{1/2}$ but similar t_{max} indicating that the lipid coating allows maintenance of therapeutic concentration of PTX in lung tissue over an extended period. The results suggests that Lipo-NCs was suitable for localized pulmonary delivery of PTX, providing prolonged and efficient therapeutics effect with minimal off-site distribution. The outcomes were similar to earlier studies on lipid nanoparticles delivered by

intratracheal inhalation, which demonstrated a longer drug retention in the lung and, thus, more efficient drug delivery to the lungs in comparison to intravenous administration (Li et al., 2020b).

4.7. Summary

Inhalable nanoparticles in solid-state dry powders for pulmonary drug delivery provide distinct advantages and represent an intriguing new area of research. Nanocrystals can be produced as a dry powder for inhalation (DPIs) to deliver high doses of drug to the lungs, owing to their high payload and stability to the shear stress of aerosolization force. Furthermore, lipid-coated nanocrystals can be formulated to improve the drug accumulation and retention in lung. The present work involved the fabrication of paclitaxel nanocrystals using hydrophilic marine biopolymer fucoidan as a stabilizer. Thereafter, fabricated nanocrystals (FPNC) were surface-modified with phospholipid to give lipid-coated nanocrystals (Lipo-NCs). The nanocrystals were highly stable, monodispersed, exhibited a high loading potential and were robust to dilution. Prepared nanocrystals were lyophilized to obtain a dry powder of FPNC and Lipo-NCs, and were stable during storage. Different techniques like FTIR, XRD, DSC, and XPS were used for solid state characterization of FPNC and Lipo-NCs dry powder and confirmed successful formation of fucoidan stabilized nanocrystals further coated with phospholipid. Solid-state NMR and circular dichroism were also employed as new techniques to confirm the change in conformation of PTX when fabricated as nanocrystals, thereby confirming successful stabilization of crystalline PTX by amorphous fucoidan. The results were in agreement with other spectroscopic techniques. BET, wettability and saturation solubility study revealed increased effective surface owing to submicron size of nanocrystals and hydrophilic fucoidan stabilized surface that increased the aqueous solubility of PTX. The in-vitro performance of

nanocrystals dry powder was evaluated by in-vitro drug release and drug diffusion study in simulated lung study. FPNC showed drug release and mucus diffusion at a higher rate, followed by Lipo-NCs and pure PTX. Powder flow analysis and in-vitro aerosolization investigation of nanocrystals DPIs showed excellent flow property and good aerosolization performance for both FPNC as well as Lipo-NCs, suitable for high dispersion and deep lung deposition. The pharmacokinetic and biodistribution study also confirmed the high drug distribution in lung by FPNC and Lipo-NCs than pure PTX. Nanocrystals reduced the drug distribution to other major organs like liver, kidney spleen and heart. The highest drug retention in lung was observed with Lipo-NCs followed by FPNC and pure PTX.

4.8. Conclusion

In conclusion, prepared lipid-coated nanocrystals were ideal for pulmonary administration as a dry powder for inhalation to achieve maximum drug localization in the lungs, serving as a novel formulation for more effective and extended therapeutic effect with minimal off-target distribution and avoiding systemic side effects.